Two-photon production of dilepton pairs in peripheral heavy ion collisions

Spencer R. Klein
Lawrence Berkeley National Laboratory, Berkeley, California 94720, USA

(Received 12 January 2018; published 10 May 2018)

The STAR collaboration has observed an excess production of e^+e^- pairs in relativistic heavy ion collisions, over the expectations from hadronic production models. The excess pairs have transverse momenta $p_T < 150$ MeV/c and are most prominent in peripheral gold-gold and uranium-uranium collisions. The pairs exhibit a peak at the J/ψ mass, but include a wide continuum, with pair invariant masses from 400 MeV/c^2 up to 2.6 GeV/c^2. The ALICE Collaboration observes a similar excess in peripheral lead-lead collisions, but only at the J/ψ mass, without a corresponding continuum. This paper presents a calculation of the cross section and kinematic for two-photon production of e^+e^- pairs, and find general agreement with the STAR data. The calculation is based on the STARlight simulation code, which is based on the Weizsäcker-Williams virtual photon approach. The STAR continuum observations are compatible with two-photon production of e^+e^- pairs. The ALICE analysis required individual muon p_T be greater than 1 GeV/c; this eliminated almost all of the pairs from two-photon interactions, while leaving most of the J/ψ decays.

DOI: 10.1103/PhysRevC.97.054903

I. INTRODUCTION

Two-photon collisions were extensively studied at e^+e^- colliders, where each lepton emitted a photon. These reactions were used to study a variety of hadronic final states and also four-lepton final states [1,2]. More recently, they have been studied in ultraperipheral collisions (UPCs) of relativistic heavy ions. UPCs are collisions where the nuclei physically miss each other (impact parameter b greater than twice the nuclear radius R_A), but interact electromagnetically. The very strong electromagnetic fields, which emanate from highly charged heavy ions lead to large cross sections for photonuclear and two-photon interactions [3–5]. Two-photon interactions of interest include e^+e^- production in strong fields and light-by-light scattering [6]. The reaction $\gamma\gamma \to l^+l^-$ has been studied in UPCs by the STAR [7], ATLAS [8], ALICE [9], and CMS [10] collaborations, and good agreement with lowest-order quantum electrodynamics predictions was seen.

Recently, the STAR experiment observed an excess of e^+e^- pairs, produced at small transverse momentum ($p_T <$ 150 MeV/c) in peripheral gold-gold and uranium-uranium collisions at a center of mass energies of 200 GeV/nucleon pair and 193 GeV/nucleon pair, respectively [11,12]. The e^+e^- invariant mass spectrum of the low p_T excess shows a significant peak at the J/ψ, but also includes a continuum component in the mass range from 400 MeV–2.6 GeV. The signal is most prominent in more peripheral collisions (60% to 80% centrality) than in those with smaller impact parameters. Here, 0% centrality is a head-on collision with impact parameter $b = 0$, while 100% centrality is a grazing collision with $b = 2R_A$.

ALICE has also reported on an excess of $\mu^+\mu^-$ pairs at low p_T [13] in very peripheral (70–90% centrality) lead-lead collisions at a center-of-mass energy of 2.76 TeV/nucleon pair. The peak data are consistent with J/ψ photoproduction [14–16], but they do not see significant continuum production.

The STAR and ALICE J/ψ rates and p_T spectra are in agreement with expectations from photoproduction, including the cutoff at very low p_T due to interference between photoproduction for photons coming from the opposite directions [17,18]. However, the broad STAR mass continuum does not seem compatible with vector meson photoproduction. The featureless mass distribution and limitation to low p_T are both very suggestive of two-photon production of e^+e^- pairs.

In this paper, I calculate the rates and kinematic distributions for two-photon production of e^+e^- pairs in peripheral hadronic collisions, and show that it is generally compatible with the STAR observation and ALICE nonobservation of continuum production at low p_T. The results provide a basis for a more detailed comparison between the data and two-photon theory.

II. METHODS

The cross sections and kinematic distributions for $\gamma\gamma \to e^+e^-$ in peripheral collisions are calculated using the photon flux predicted by the Weizsäcker-Williams method, and the lowest-order Breit-Wheeler cross section for $\gamma\gamma \to e^+e^-$. For ultrarelativistic particles, the photon flux at a perpendicular distance b from an emitting nucleus with nuclear charge Z is [4,5,19]

$$N(k,b) = \frac{Z^2\alpha}{\pi^2}\frac{k}{(\hbar c\gamma)^2}K_1(x)^2, \tag{1}$$

where k is the photon energy, $x = kb/\gamma\hbar c$, γ is the ion Lorentz boost, $\alpha \approx 1/137$ is the electromagnetic fine structure constant, and $K_1(x)$ is a modified Bessel function.

The cross section depends on the overlap of the photon fluxes, integrated over all possible transverse positions for the two ions and the location of the photon-photon interaction. This can be simplified to a three-dimensional integral over the distance from the first ion to the interaction site, b_1, the distance from the second ion site, b_2, and the angle ϕ between the two ion-interaction site vectors [20]. For peripheral collisions, the ion-ion impact parameter range is restricted to match a desired centrality bin: $b_{\rm min} < |b| < b_{\rm max}$. The cross section to produce a final state W from photons with energy k_1 and k_2 is

$$\sigma = \int_{R_A}^{\infty} \pi b_1 d^2 b_1 \int_{R_A}^{\infty} \pi b_2 db_2 \int_0^{2\pi} d\phi N(k_1,b_1)N(k_2,b_2) \sigma(k_1k_2 \to W)\theta(b_{\rm min} < |b_1 - b_2| < b_{\rm max}), \tag{2}$$

where the θ function is 1 when the inequality is satisfied, and 0 otherwise.

This approach assumes that the photons come from the electromagnetic fields of the entire nucleus, moving at the full beam velocity. Since the fields at time t are evaluated based on the nucleus configuration at a retarded time $\tau = t - |b_i|/\gamma c$ [21], this assumption should be satisfied. This approach also assumes that the photon flux is zero within the emitting nucleus (i.e., for $|b| < R_A$). The inclusion of interactions occurring within one of the nuclei would slightly increase the calculated cross section, with the size of the increase rising with increasing pair mass.

The final-state pair mass M_{ll} is given by the two-photon center of mass energy W. The photon energies map into W and rapidity y via $W = M_{ll} = 2\sqrt{k_1k_2}$ and $y = 1/2 \ln(k_1/k_2)$.

The cross section to produce pairs of leptons with lepton mass m is the Breit-Wheeler cross section [22]:

$$\sigma(\gamma\gamma \to l^+l^-) = \frac{4\pi\alpha^2}{W^2}\left[\left(2 + \frac{8m^2}{W^2} - \frac{16m^4}{W^4}\right)\ln\left(\frac{W + \sqrt{W^2 - 4m^2}}{2m}\right) - \sqrt{1 - \frac{4m^2}{W^2}}\left(1 + \frac{4m^2}{W^2}\right)\right]. \tag{3}$$

The angular distribution of the decay electrons also follows Breit-Wheeler, with the leptons preferentially emitted in the forward and backward directions:

$$G(\theta) = 2 + 4\left(1 - \frac{4m^2}{W^2}\right)\frac{\left(1 - \frac{4m^2}{W^2}\right)\sin^2(\theta)\cos^2(\theta) + \frac{4m^2}{W^2}}{\left[1 - \left(1 - \frac{4m^2}{W^2}\right)\cos^2(\theta)\right]^2}, \tag{4}$$

where θ is the angle between the beam direction and one of the leptons, in the lepton-lepton center of mass frame.

The pair p_T is the vector sum of the photon k_T; the photon k_T comes from the Weizsäcker-Williams approach [17,23]:

$$\frac{dN}{dk_T} = \frac{2F^2(k^2/\gamma^2 + k_T^2)k_T^3}{(2\pi)^2\left((k/\gamma)^2 + k_T^2\right)^2}, \tag{5}$$

where F is the nucleon form factor, per Ref. [24]. The individual lepton p_T includes contributions from this initial $\gamma\gamma$ p_T, plus the transverse kick acquired from the nonzero θ in Eq. (4).

The calculations are done in the framework of the STARlight Monte Carlo [19,24]. I modified STARlight to limit the range of integration in impact parameter to a user-selectable range, regardless of whether the two nuclei overlap or not, as shown in Eq. (2); this code is publicly available in the trunk of STARlight [25]. STARlight has been extensively compared with UPC data, with good agreement found for $\gamma\gamma \to l^+l^-$, with data from STAR [7], ATLAS [8], ALICE [9], and CMS [10] collaborations. There is a discrepancy at small pair p_T where the equivalent photon approximation predicts an overabundance of pairs, compared to both a lowest-order quantum electrodynamics (QED) calculation and data [7]. ATLAS also sees a small tail of events with larger pair p_T; the collaboration notes that this might be background, or it might be from the two-photon signal. Also, STARlight assumes that nuclei are spherical. Uranium is aspherical; this introduces an additional uncertainty in the uranium-uranium calculations.

III. RESULTS

Most of the $\gamma\gamma \to ee$ cross section is for near-threshold pairs, which are not visible in existing detectors. These calculations focus on experimentally accessible interactions, so consider only pairs with invariant masses above 400 MeV/c^2. Results are presented for five different experimental conditions: 60–80% centrality, 40–60% centrality, and 10–40% centrality Au-Au collisions at a center-of-mass (CM) energy of 200 GeV/nucleon, 60–80% U-U collisions at a slightly lower CM energy, 193 GeV/nucleon (all at RHIC), and 60–80% Pb-Pb collisions at a center of mass energy of 2.76 TeV/nucleon at the LHC. These calculations are for a central detector, following the STAR acceptance [11]. As noted below, the ALICE forward muon spectrometer has little acceptance for two-photon production of dimuons, and an ALICE study in the central region would likely have a similar acceptance to STAR.

The collaborations report impact parameter range in terms of collision centrality. A Monte Carlo Glauber calculation [26] is used to convert from the reported centralities into impact parameters. The calculation finds cross sections of 6.8 barns for Au-Au collisions at RHIC, 7.8 barns for U-U collisions at RHIC [27], and 7.6 barns for Pb-Pb collisions at the LHC at a center-of-mass energy of 2.76 TeV/nucleon pair, all with errors that are negligible compared to other uncertainties in the overall calculation. These cross sections are 4–8% lower than some other results [28], likely because the calculation uses slightly lower inelastic proton-proton cross sections than other works. I then use a simple black-disk model to convert from centrality to impact parameter range, so 100% centrality corresponds to $b_{\rm max} = \sqrt{\sigma_{\rm had}/\pi}$. Table I shows the centrality regions and hadronic cross sections for those centralities.

Figure 1 shows the rapidity distribution $d\sigma/dy$ for 60–80% centrality collisions of gold and uranium at RHIC and lead at the LHC for $M_{ee} > 0.4$ GeV/c^2. Because the distribution is almost independent of centrality, only one RHIC curve is shown. The integrated cross sections are 6.7 mb, 8.7 mb, and 24.2 mb for gold, uranium, and lead, respectively. The LHC cross section is much larger and covers a much wider rapidity range than the RHIC curves, because of the higher beam energy. The uranium cross section is about 36% larger than that for gold, less than the 54% increase expected from the naive Z^4 scaling. Uranium nuclei are larger than gold nuclei, and the per-nucleon collision energy was a bit lower, so the photon flux, Eq. (1) is cut off at about 10% lower energy than

TABLE I. Ions and centralities, impact parameters, and cross sections for two-photon production of lepton pairs. The centralities were chosen to match the STAR analysis. The table also gives the calculated photoproduction cross section (within the given constraints on pair mass and rapidity), the fraction of those events that pass the individual lepton kinematic cuts, and the fraction of the hadronic events in that centrality that should contain a visible (satisfying the pair and individual lepton constraints) lepton pair.

Ion/Centrality	b range	σ_{had}	σ_{ll} (restr.)	% satisfying $l^{\pm}$ criteria	$\#_{visible\ ll}$ hadronic event
60–80% RHIC Au-Au	11.4–13.2 fm	1.36 b	3.7 mb	3.3%	8.9×10^{-5}
40–60% RHIC Au-Au	9.4–11.6 fm	1.36 b	3.8 mb	3.3%	9.2×10^{-5}
10–40% RHIC Au-Au	4.8–9.4 fm	2.04 b	6.4 mb	3.3%	1.03×10^{-4}
60–80% RHIC U-U	14.1–15.8 fm	1.56 b	5.2 mb	3.3%	1.01×10^{-4}
60–80% LHC Pb-Pb	13.0–14.7 fm	1.51 b	6.4 mb	3.5%	1.4×10^{-4}

for gold. The cutoff is also evident in the rapidity distribution, which is slightly narrower than for gold-gold.

Figure 2 shows the p_T spectra for the individual leptons for the three systems, along with, for comparison, the lepton p_T from photoproduction of J/ψ in gold-gold ultraperipheral collisions at RHIC [17,24,29]. The leptons from $\gamma\gamma \rightarrow e^+e^-$ are peaked at very low p_T, in sharp contrast to the leptons from J/ψ decays. This difference immediately shows why the ALICE forward muon spectrometer cut on muon $p_T > 1$ GeV/c almost completely eliminates pairs from $\gamma\gamma$ interactions while retaining the pairs from coherent J/ψ photoproduction, even though the two reactions have not dissimilar pair p_T spectra. The p_T spectra from the three $\gamma\gamma$ channels are similar, with small changes due to the per-nucleon collision energy and size of the nuclei.

We now turn to calculations of cross sections within the STAR acceptance: pairs with pair mass $M_{ee} > 0.4$ GeV/c^2 and rapidity $|y_{ee}| < 1$. STAR also requires that the individual leptons satisfy $p_{T,e} > 200$ MeV/c and pseudorapidity $|\eta_e| < 1$. Table I shows the cross sections for five different beam species, energy, and centrality conditions, for hadronic interactions, the cross sections for $\gamma\gamma \rightarrow e^+e^-$ within the pair rapidity and pair mass range, the probability for those events to also satisfy the individual lepton pseudorapidity and p_T cuts, and, finally, the number of pairs within the full STAR acceptance per hadronic collisions. The hadronic cross section is the total hadronic cross section times the width of the centrality bin.

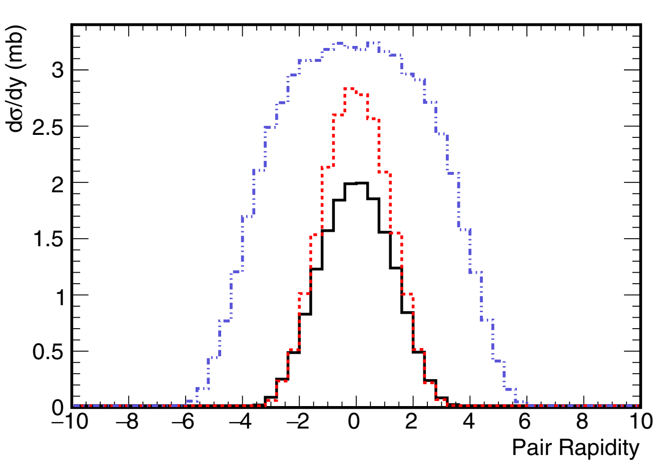

FIG. 1. $d\sigma/dy$ for $\gamma\gamma \rightarrow e^+e^-$ with pair mass more than 400 MeV/c^2, for 60–80% centrality gold-gold (solid black histogram) and uranium-uranium (dashed red histogram) at RHIC and lead-lead collisions at the LHC (dot-dashed blue line).

For a fixed condition and acceptance, the restricted two-photon cross section depends mostly on the width of the centrality bin. The cross section is higher for Pb-Pb collisions, because of the higher LHC collision energy; the increase in $\gamma\gamma$ cross section with energy is much faster than the rise in hadronic cross section. This increase is reflected in the higher number of visible ee pairs for Pb-Pb collisions than for the lower-energy RHIC systems.

The restricted cross section is 40% larger for U-U cross sections than for Au-Au collisions. This is again less than the 54% increase expected from the Z^4 scaling, but larger than the increase in the all-rapidity cross section, because, for the heavier nucleus, production is more concentrated at small $|y|$.

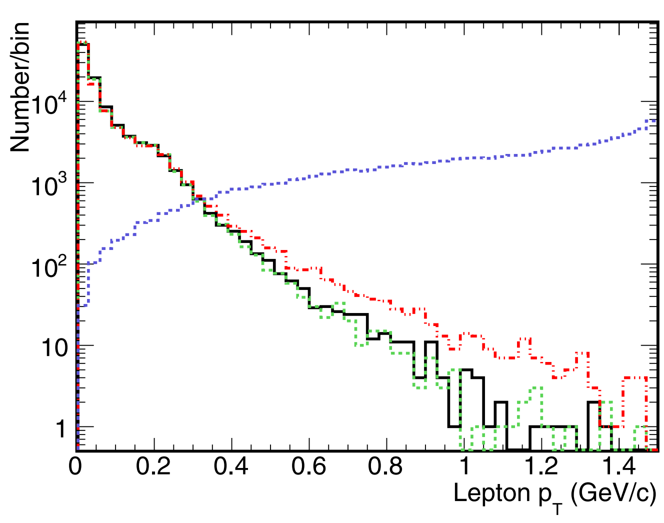

FIG. 2. Individual lepton p_T for Au-Au (solid black histogram) and U-U (dashed green histogram) at RHIC and Pb-Pb collisions at the LHC (dot-dashed red histogram), along with the lepton p_T from photoproduction of J/ψ in Au-Au ultraperipheral collisions at RHIC (dotted blue line). The histograms are each normalized to contain 10^5 events total, so that the differences in spectral shape are visible. The y axis gives the number of events in each 30 MeV/c wide bin.

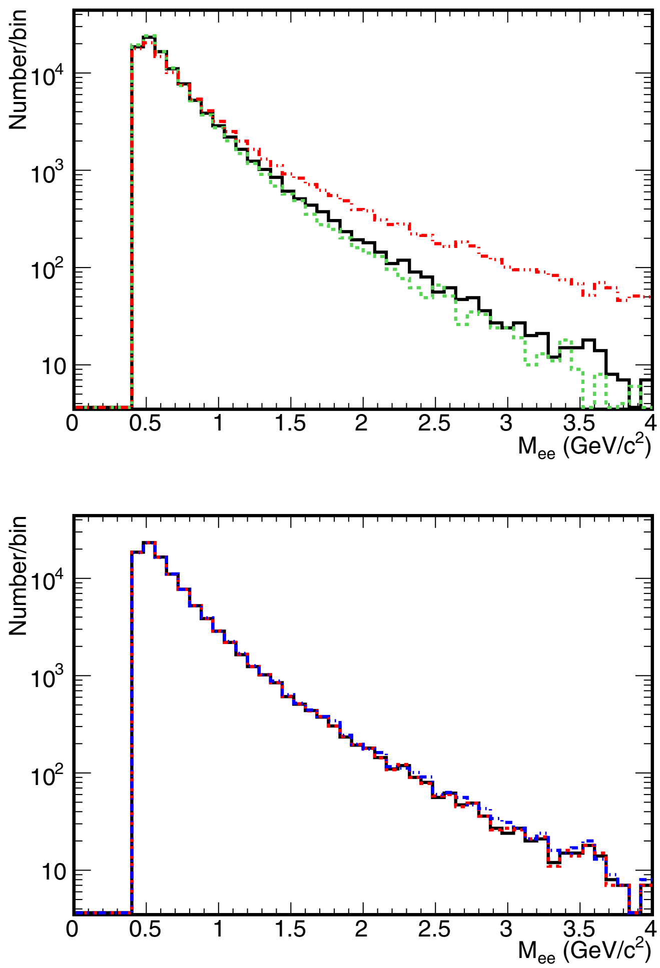

FIG. 3. Pair invariant mass spectra for (top) Au-Au (black solid histogram), U-U (green dashed histogram), and Pb-Pb (red dot-dashed histogram) and (bottom) 60–80% centrality (black solid histogram), 40–60% centrality (red dashed histogram), and 10–40% centrality (blue dot-dashed histogram). The bottom three histograms are indistinguishable. The histograms are each normalized to contain 10^5 events total, so that the differences in spectral shape are visible. The y axis gives the number of events in each 80 MeV/c^2 wide bin.

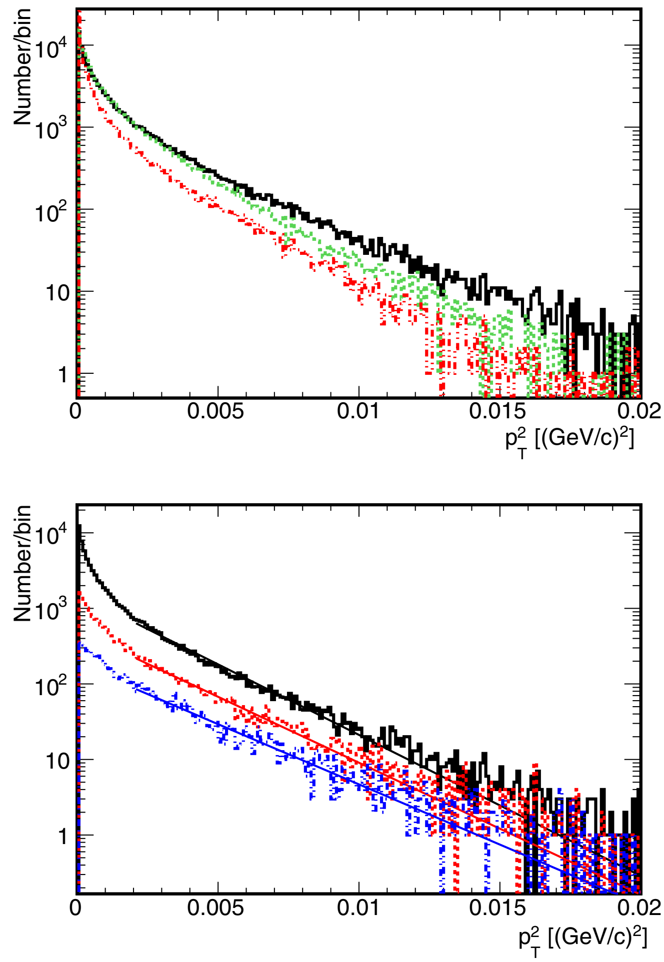

FIG. 4. Pair p_T^2 spectra for (top) Au-Au (black solid histogram), U-U (green dashed histogram), and Pb-Pb (red dot-dashed histogram) and (bottom) for three invariant mass ranges: 0.4 to 0.76 GeV/c^2 (black solid histogram), 0.76–1.2 GeV/c^2 (red dashed histogram), and 1.2–2.6 GeV/c^2 (blue dot-dashed histogram). The histograms are each normalized to contain 10^5 events total, so that the differences in spectral shape are visible. The bottom three histograms show a clear mass ordering. They are normalized based on the relative number of events expected in each mass bin. The lines in the bottom plot are fits to Eq. (6) in the displayed region, as discussed in the text. In both panels, the y axis gives the number of events in each 0.0001 (GeV/c)^2 wide bin.

The fraction of lepton pairs that pass the individual lepton cuts is about 3.4%, almost independent of the collision conditions, with only a small rise for the higher-energy Pb-Pb collisions. This acceptance is so low because, per Eq. (4), the pairs from two-photon interactions prefer a forward-backward geometry, and so avoid the central region.

Figure 3 shows the pair invariant mass distributions for events within the STAR acceptance. The Pb-Pb data spectrum is harder than the Au-Au and U-U distributions, because of the higher beam energy. The U-U spectrum is slightly softer than the Au-Au distribution, because of the slightly larger nuclear size and lower per-nucleon collision energy. The shape of these distributions are similar to the STAR data presented in Ref. [11]; The number of events drops by roughly a factor of 10 as the pair mass doubles from 0.5–1.0 GeV, in at least rough agreement with the STAR data.

Figure 4 shows the distribution of lepton pair p_T^2 for the three species (top), and the three Au-Au centralities (bottom). A significant upturn is seen for $p_T^2 < 0.002$ (GeV/c)^2, while at higher energies, the distribution looks quasiexponential. The p_T^2 scale is lowest for Pb-Pb because, for a fixed photon energy k, the photon k_T drops with increasing ion energy. The U-U distribution is slightly softer than the Au-Au spectrum because the larger nuclear size softens the energy distribution.

At low p_T, the equivalent photon approach used here differs from a lowest-order QED calculation, which predicts a drop off at low p_T. Data from $\gamma\gamma \rightarrow ee$ in ultraperipheral collisions also does not show this increase [7]. The peak of the pair p_T distribution scales roughly as $\sqrt{1.5M_{ee}}/\gamma$ [19]. In Ref. [7], the data diverged from the equivalent photon calculation for

$p_T < 20$ MeV/c, for a sample with $M_{ee} > 140$ MeV/c^2. If the $\sqrt{M_{ee}}$ scaling holds, the calculated p_T^2 spectrum should be acceptable for $p_T > 35$ MeV/c, or $p_T^2 > 0.001\,(\text{GeV}/c)^2$.

Following the STAR Collaboration [11], these curves are fit to exponential distributions,

$$\frac{dN}{dp_T^2} = a \exp\left(-bp_T^2\right) \qquad (6)$$

for events in three mass regions, 0.4–0.76 GeV/c^2, 0.76–1.2 GeV/c^2, and 1.2–2.6 GeV/c^2. The fit region was chosen to avoid the upturn at low p_T: $0.002\,(\text{GeV}/c)^2 < p_T^2 < 0.02\,(\text{GeV}/c)^2$. The fits are shown with the colored lines in the bottom panel of Fig. 4. The slopes are $430 \pm 4\,(\text{GeV}/c)^{-2}$, $402 \pm 6\,(\text{GeV}/c)^{-2}$, and $367 \pm 9\,(\text{GeV}/c)^{-2}$ for the low, medium, and high mass regions, respectively. These numbers are near the upper end of the uncertainty ranges reported by STAR [11], but the trend with increasing mass agrees well with the data. It should be noted that STAR used a significantly different fit range, $0.0004\,(\text{GeV}/c)^2 < p_T^2 < 0.0064(\text{GeV}/c)^2$. That range overlaps with the low-p_T upturn in Fig. 4 and would have led to significantly larger fit slopes, in disagreement with the STAR data. Even for the chosen range, the slope depends slightly on the chosen fit range.

These slope differences are not surprising. For $k_T \gg k/\gamma$, dN/dk_T from Eq. (5) scales as $F^2(k_T^2)/k_T$. This naively implies similar slopes, but k scales linearly with pair mass (with some rapidity dependence), so the location of the transition to the $k_T \gg k/\gamma$ varies with pair mass. The contribution to pair p_T from θ, Eq. (3), should also scale with pair mass, with, for the lepton pseudorapidity cut, a significant dependence on the pair rapidity.

Similar fits were made to the Au-Au, U-U and Pb-Pb distributions, over the range 400 MeV–4 GeV^2. They yielded slopes of $404 \pm 3\,(\text{GeV}/c)^{-2}$, $502 \pm 4\,(\text{GeV}/c)^{-2}$, and $483 \pm 5\,(\text{GeV}/c)^{-2}$, respectively. The Au-Au and U-U points have a similar trend to the STAR fits, albeit with a larger separation between the two slopes.

IV. CONCLUSIONS

Two-photon production of lepton pairs in ultrarelativistic collisions is a well-understood process, studied in many ultraperipheral collision analyses. In this paper, I have studied the two-photon production of lepton pairs in peripheral collisions, and found that it describes the general characteristics of the STAR observations of a continuum excess of e^+e^- pairs at low p_T quite well. ALICE did not observe this continuum; this is expected because of the required minimum p_T for muons to be observable in their forward muon spectrometer. However, it should be visible in a future ALICE midrapidity study if a low enough lepton p_T cut can be applied.

ACKNOWLEDGMENTS

I thank Jamie Dunlop, Michael Lomnitz, Lijuan Ruan, Shuai Yang, Wangmei Zha, and Zhangbu Xu for useful discussions. This work was funded by the US Department of Energy under Contract No. DE-AC-76SF00098.

[1] V. M. Budnev, I. F. Ginzburg, G. V. Meledin, and V. G. Serbo, Phys. Rept. **15**, 181 (1975).
[2] H. Kolanowski, *Two-Photon Physics at e^+e^- Storage Rings* (Springer-Verlag, Berlin, 2006).
[3] A. J. Baltz *et al.*, Phys. Rep. **458**, 1 (2008).
[4] C. A. Bertulani, S. R. Klein, and J. Nystrand, Ann. Rev. Nucl. Part. Sci. **55**, 271 (2005).
[5] G. Baur, K. Hencken, D. Trautmann, S. Sadovsky, and Y. Kharlov, Phys. Rept. **364**, 359 (2002).
[6] M. Aaboud *et al.* (ATLAS Collaboration), Nature Phys. **13**, 852 (2017).
[7] J. Adams *et al.* (STAR Collaboration), Phys. Rev. C **70**, 031902 (2004).
[8] M. Dyndal (ATLAS Collaboration), Nucl. Phys. A **967**, 281 (2017).
[9] E. Abbas *et al.* (ALICE Collaboration), Eur. Phys. J. C **73**, 2617 (2013).
[10] V. Khachatryan *et al.* (CMS Collaboration), Phys. Lett. B **772**, 489 (2017).
[11] S. Yang for the STAR Collaboration, presented at Quark Matter 2017, https://indico.cern.ch/event/433345/contributions/2373720/.
[12] W. Zha for the STAR Collaboration, presented at Quark Matter 2017, https://indico.cern.ch/event/433345/contributions/2358104/.
[13] J. Adam *et al.* (ALICE Collaboration), Phys. Rev. Lett. **116**, 222301 (2016).
[14] M. Klusek-Gawenda and A. Szczurek, Phys. Rev. C **93**, 044912 (2016).
[15] W. Zha *et al.*, Phys. Rev. C **97**, 044910 (2018).
[16] W. Shi, W. Zha, and B. Chen, Phys. Lett. B **777**, 399 (2018).
[17] S. R. Klein and J. Nystrand, Phys. Rev. Lett. **84**, 2330 (2000).
[18] B. I. Abelev *et al.* (STAR Collaboration), Phys. Rev. Lett. **102**, 112301 (2009).
[19] A. J. Baltz, Y. Gorbunov, S. R. Klein, and J. Nystrand, Phys. Rev. C **80**, 044902 (2009).
[20] G. Baur and L. G. Ferreira Filho, Nucl. Phys. A **518**, 786 (1990).
[21] J. D. Jackson, *Classical Electrodynamics*, 2nd edition (John Wiley & Sons, New York, 1975).
[22] S. J. Brodsky, T. Kinoshita, and H. Terazawa, Phys. Rev. D **4**, 1532 (1971).
[23] M. Vidovic, M. Greiner, C. Best, and G. Soff, Phys. Rev. C **47**, 2308 (1993).
[24] S. R. Klein, J. Nystrand, J. Seger, Y. Gorbunov, and J. Butterworth, Comput. Phys. Commun. **212**, 258 (2017).
[25] STARlight is available at https://starlight.hepforge.org/.
[26] C. Loizides, J. Kamin, and D. d'Enterria, arXiv:1710.07098 [nucl-ex].
[27] D. d'Enterria (private communication), 2017.
[28] W. Fischer, A. J. Baltz, M. Blaskiewicz, D. Gassner, K. A. Drees, Y. Luo, M. Minty, P. Thieberger, M. Wilinski, and I. A. Pshenichnov, Phys. Rev. C **89**, 014906 (2014).
[29] S. R. Klein and J. Nystrand, Phys. Rev. C **60**, 014903 (1999).